Light Levitated Geostationary Cylindrical Orbits are Feasible

Shahid Baig[*]and Colin R. McInnes[†]

University of Strathclyde, Glasgow, G1 1XJ, Scotland, UK.

This paper discusses a new family of non-Keplerian orbits for solar sail spacecraft displaced above or below the Earth's equatorial plane. The work aims to prove the assertion in the literature that displaced geostationary orbits exist, possibly to increase the number of available slots for geostationary communications satellites. The existence of displaced non-Keplerian periodic orbits is first shown analytically by linearization of the solar sail dynamics around a geostationary point. The full displaced periodic solution of the nonlinear equations of motion is then obtained using a Hermite-Simpson collocation method with inequality path constraints. The initial guess to the collocation method is given by the linearized solution and the inequality path constraints are enforced as a box around the linearized solution. The linear and nonlinear displaced periodic orbits are also obtained for the worst-case Sun-sail orientation at the solstices. Near-term and high-performance sails can be displaced between 10 km and 25 km above the Earth's equatorial plane during the summer solstice, while a perforated sail can be displaced above the usual station-keeping box (75 × 75 km) of nominal geostationary satellites. Light-levitated orbit applications to Space Solar Power are also considered.

I.   Introduction

An ideal solar sail consists of a large, lightweight reflector and generates thrust normal to its surface from incident and reflected solar radiation. Solar sails are capable of a wide class of orbits beyond those of traditional conic section Keplerian orbits. In fact, solar sails are well-suited for non-Keplerian orbits (NKO), since they can provide propellantless thrust continuously. The nearest term NKO enabled by solar sails are the Heliostorm mission[1] at a sub-L_1 point for increased warning time of solar storms, and the Geosail mission[2–4] in Earth orbit to explore the geomagnetic tail with long residence times.

Displaced non-Keplerian orbits for solar sails have been considered by various authors for applications in two and three body problems. Forward[5] proposed fixed points (artificial equilibria) high above the ecliptic plane towards the night-side of the Earth for high latitude communications and McInnes[6,7] proposed artificial equilibria towards the day side of the Earth for real-time polar imaging. Both are examples of one-year NKO in the Sun-Earth three-body problem. McInnes[8] and Simo and McInnes[9] investigated displaced orbits above L_2 for lunar far side communication and Ozimek at el.[10] find displaced orbits below L_1 and L_2 for lunar south pole coverage as examples of lunar synodic month NKO in the Earth-Moon three body problem. McInnes and Simmons[11] found families of Sun-centered circular NKO (orbit period as a free parameter) for solar physics applications, and one year orbit synchronous with the Earth for space weather missions as examples of two-body displaced NKO. McInnes and Simmons[12] also found families of planet-centered circular NKO behind the planet in the anti-Sun direction to observe the full 3D structure of the geomagnetic tail. Two approaches are used to generate solar sail NKO. In the first approach Forward[5] and McInnes[7] formulate three-body dynamics, and McInnes and Simmons[11,12] formulate two-body dynamics in the rotating frame to look for artificial equilibria and obtain NKO when viewed in an inertial frame, whereas in the second approach McInnes,[8] Simo and McInnes[9] and Ozimek at el.[10] investigate NKO in the rotating frame of the Earth-Moon three body system because of the nonautonomous dynamics of the problem. In this paper, the second approach is adopted and formulates the Earth-sail system as a two-body problem in the presence

---

*PhD Candidate, Advanced Space Concepts Laboratory, Department of Mechanical Engineering, shahid.baig@strath.ac.uk

†Professor, Advanced Space Concepts Laboratory, Department of Mechanical Engineering, colin.mcinnes@strath.ac.uk, member AIAA

American Institute of Aeronautics and Astronautics

of solar radiation pressure to investigate the NKO (not equilibria) in the Earth rotating frame around geostationary points.

The solar sail characteristic acceleration required to enable these NKO is a function of the local gravitational acceleration. Ozimek et al.[10] describe NKO possible with a characteristic acceleration of $0.57 - 1.57$ mms^{-2} envisioned with current sail technologies, McInnes[13] mentions NKO for high performance sails with a characteristic acceleration of 6 mms^{-2}, and Forward[14] suggests perforated sails for 'levitation' above geostationary orbit.

A satellite in geostationary orbit has continuous communication with a point on the ground since both the satellite and ground station move with the same (Earth) angular velocity, thus greatly simplifying the ground antenna tracking problem. Orbital positions on geostationary orbit (a single orbit) are defined by longitude and a station-keeping box of order 75×75 km or 150×150 km is assigned with respect to its original central (longitude) position,[15] within which the satellite is maintained. However, various slots (longitudes) along geostationary orbit are already crowded. In order to increase the number of slots over a particular longitude, Forward[14, 16] first proposed the idea to 'levitate' the sail above or below the nominal geostationary orbit. He tried to achieve 'equilibria' in the Earth fixed rotating frame to form the NKO in an inertial frame. By tilting the solar sail, Forward[14, 16] uses a component of sail acceleration perpendicular to the Earth's equatorial plane to 'levitate' the sail above or below the Earth's equatorial plane. However, Fischer and Haerting,[17] in their paper 'Why light-levitation geostationary cylinderical orbits are not feasible', and later Kolk[18] claim such light-levitation is not possible, as the component of sail acceleration neglected by Forward[14, 16] parallel to the Earth's equatorial plane does not allow for 'equilibria'. In this paper, this neglected parallel component is used to generate a periodic orbit, thus a NKO for an observer in the Earth fixed rotating frame at a geostationary point exists. It is first shown from linear analysis the existence of such NKO. The nonlinear analysis is adopted from Ozimek et al.[10, 19] who find displaced periodic orbits for continuous lunar south pole coverage from a collocation scheme using (partly) a numerical Jacobian matrix and a minimum elevation angle constraint. However, this paper computes the displaced periodic orbits in the nonlinear analysis using an analytical Jacobian and a box around the linearized NKO as a path constraint. While the existence of levitated geostationary orbits is demonstrated, as proposed by Forward,[14, 16] only modest displacements are found due to the large in-plane component of sail acceleration. Recently, Takeichi et al.[20] propose a solar power satellite system in which reflectors orbiting in levitated geostationary orbits (typically at ± 2 km levitation) are used to concentrate Sun-light to microwave generator-transmitters orbiting separately at geostationary orbit and in-between the reflectors. It is shown that these orbits are feasible.

The paper is arranged as follows: In Sec. II the nonlinear equations of motion in the Earth rotating frame are defined for a solar sail above the Earth's equatorial plane with the Sun-line assumed to be in the Earth's equatorial plane. In Sec. III the solution to the linearized equations of motion around a geostationary point are considered. It is found that NKO exist at linear order. This linear solution will act as an initial guess for finding the NKO with the nonlinear equations of motion. In Sec. IV a collocation scheme is described which adjusts the sail orientation for handling the nonlinearities of the Earth's gravity around the geostationary point to give displaced periodic solutions to the full nonlinear non-autonomous system. In Sec. V a linear analysis is conducted at the summer and winter solstices, when the Sun-line is at maximum excursion from the Earth's equatorial plane. In Sec. VI the collocation scheme is used to generate displaced periodic orbits at the summer solstice. In Sec. VII light-levitated geostationary orbits for the reflectors of solar power satellite systems are shown.

II.   Equations of Motion

A geostationary satellite (shown as geostationary point in Fig.1) orbits the Earth in the equatorial plane at Earth's rotational angular velocity w_e, i.e., the geostationary point moves with an orbital period equal to one sidereal day ($\tau_e = 23$ h, 56 min, 4.1 s $= 86164.1$ s). If $\mu_g = 3986004.418 \times 10^8$ m^3/s^2 denotes the gravitational parameter, then the radius r_{gs} of the geostationary point follows from

$$\sqrt{\mu_g/r_{gs}^3} = \frac{2\pi}{\tau_e} = w_e \qquad (1)$$

with the result that $r_{gs} = 42164.1696$ km. Consider two coordinate systems, Earth-centred inertial (ECI) and Earth-centred, Earth-fixed (ECEF) with common origin 'o' at the Earth's center of mass as shown in Fig. 1. The ECI system is an inertial frame with axes x_I, y_I in the equatorial plane and the z_I-axis is directed
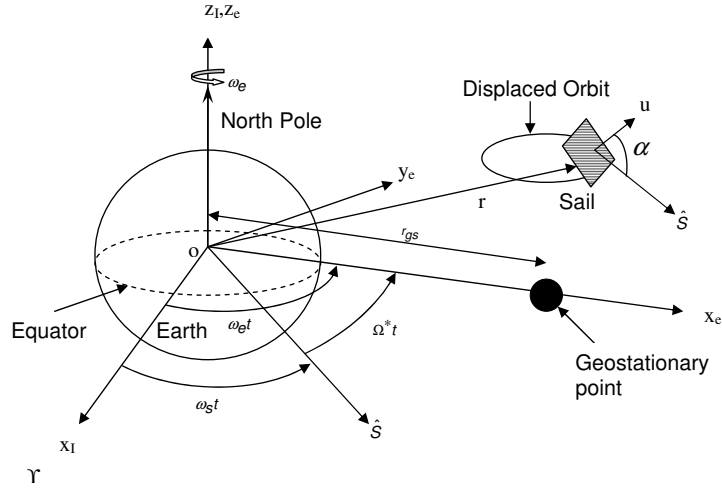
Figure 1. Two coordinate systems ECI (x_I, y_I, z_I) and ECEF (x_e, y_e, z_e) are shown. A solar sail on a displaced orbit above the equatorial plane around a geostationary point at r_{gs}, where the sun-line $\hat{S}$ is initially assumed to be in the Earth's equatorial plane.

along the Earth's spin axis. Furthermore, the x_I-axis is aligned with the vernal equinox. The ECEF system is a rotating frame which is defined by the rotating Earth with axes x_e, y_e in the Earth equatorial plane and z_e is directed along the Earth's spin axis. The angular velocity of this frame is therefore $\boldsymbol{w}_e = w_e \hat{z}_e$. In addition, the x_e-axis points to the geostationary point and is aligned with the x_I axis at $t = 0$. The units are chosen to set the gravitational parameter μ_g, the distance between the center of Earth and geostationary point r_{gs} and the magnitude of the angular velocity of the rotating frame w_e to be unity. The unit reference acceleration and unit reference time are then given by

$$a_r = w_e^2 r_{gs} = 0.224208 \quad \text{m/s}^2 \tag{2}$$

$$\tau_r = \frac{\tau_e}{2\pi} \quad \text{sec} \tag{3}$$

In this paper, an ideal solar sail and a spherically symmetric Earth are assumed. Thus, the nondimensional equation of motion in the ECEF system is given by

$$\frac{d^2\boldsymbol{r}}{dt^2} + 2\boldsymbol{\omega}_e \times \frac{d\boldsymbol{r}}{dt} + \nabla U = \boldsymbol{a} \tag{4}$$

where $\boldsymbol{r} = (x, y, z)^T$ is the position vector of the solar sail with respect to the centre of the Earth in the ECEF frame. The two-body pseudo-potential U is defined as

$$U = V + \varphi$$

where V is the potential due to the Earth's gravity and φ is the potential due to the centrifugal force in the rotating frame which are given by

$$V = -1/r \tag{5}$$
$$\varphi = -(x^2 + y^2)/2$$

The solar radiation pressure $\boldsymbol{a}$ in Eq. (4) is defined by

$$\boldsymbol{a} = a_0 (\hat{\boldsymbol{S}}(t).\boldsymbol{u})^2 \boldsymbol{u}$$

where a_0 is the sail characteristic acceleration, $\boldsymbol{u}$ is the sail normal unit vector, and $\hat{\boldsymbol{S}}(t)$ is the unit-vector in the direction of the Sun-line. As a start point, if the Sun-line direction is assumed to be in the Earth's equatorial plane, then $\hat{\boldsymbol{S}}(t)$ is given by

$$\hat{\boldsymbol{S}}(t) = \begin{pmatrix} \cos(\Omega^* t) \\ -\sin(\Omega^* t) \\ 0 \end{pmatrix} \tag{6}$$

American Institute of Aeronautics and Astronautics

where Ω^* is the nondimensional angular velocity of the ECEF-frame relative to the Sun line and calculated using

$$\Omega^* = \frac{w_e - \omega_s}{w_e} \tag{7}$$

where $\omega_s = 2\pi/(365.25 \times 86400)$ rad/s is the angular velocity of the Sun-line with respect to the inertial frame. Fig. 2 describes the sail normal $\boldsymbol{u}$ using two angles: the sail pitch angle α (out of the equatorial
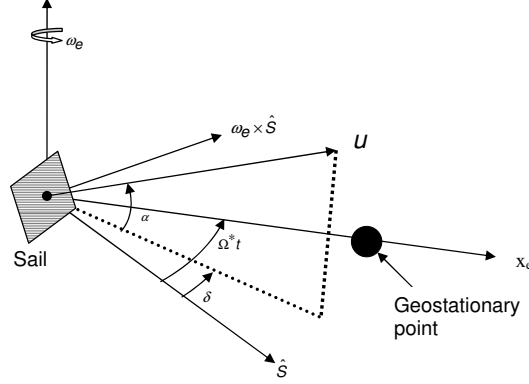

Figure 2. The sail pitch α is defined with respect to the Earth equatorial plane, while the yaw angle δ is defined with respect to the Sun-line in the equatorial plane, where the Sun-line $\hat{\boldsymbol{S}}$ is in the equator plane.

plane) and the sail yaw angle δ (in the equatorial plane). Then, the expression for $\boldsymbol{u}$ in ECEF-frame is given by

$$\boldsymbol{u} = \begin{pmatrix} \cos\alpha\cos(\Omega^*t - \delta) \\ -\cos\alpha\sin(\Omega^*t - \delta) \\ \sin\alpha \end{pmatrix} \tag{8}$$

Furthermore, the sail attitude is constrained such that $\hat{\boldsymbol{S}}(t).\boldsymbol{u} \geq 0$, so that the solar radiation-pressure acceleration can never be directed towards the Sun ($-90° < \alpha < +90°$). Thus, Eq. (4) is nonlinear due to the Earth's gravity ∇V, and nonautonomous due to the Sun-line direction $\hat{\boldsymbol{S}}(t)$ changing with time in the rotating ECEF-frame.

III.   Linearized Equations

In this section, the dynamics of the solar sail in the neighborhood of the geostationary point at $\boldsymbol{r}_{gs} = (x_e, y_e, z_e)^T = (1, 0, 0)^T$ is investigated. Perturbing Eqs. (4) such that $\boldsymbol{r} \to \boldsymbol{r}_{gs} + \delta\boldsymbol{r}$, it can be seen that

$$\frac{d^2\delta\boldsymbol{r}}{dt^2} + 2\boldsymbol{\omega}_e \times \frac{d\delta\boldsymbol{r}}{dt} + \nabla U(\boldsymbol{r}_{gs} + \delta\boldsymbol{r}) = \boldsymbol{a}(\boldsymbol{r}_{gs} + \delta\boldsymbol{r}) \tag{9}$$

where $\delta\boldsymbol{r} = (\xi, \eta, \zeta)^T$ denotes a small displacement from the geostationary point in the (x_e, y_e, z_e) directions. Now, since $\nabla U(\boldsymbol{r}_{gs}) = 0$, and $\frac{\partial \boldsymbol{a}}{\partial \boldsymbol{r}} = 0$ (the solar radiation field is assumed uniform), expanding in a Taylor series of each term about $\boldsymbol{r}_{gs}$ in Eq. (9) and retaining only the first order term in $\delta\boldsymbol{r}$, it can be seen that

$$\frac{d^2\delta\boldsymbol{r}}{dt^2} + 2\boldsymbol{\omega}_e \times \frac{d\delta\boldsymbol{r}}{dt} + K\delta\boldsymbol{r} = \boldsymbol{a} \tag{10}$$

where the matrix K is the partial derivatives of the pseudo-potential given by

$$K = \left.\frac{\partial \nabla U}{\partial \boldsymbol{r}}\right|_{\boldsymbol{r}=\boldsymbol{r}_{gs}} = \begin{pmatrix} U_{xx}^0 & 0 & 0 \\ 0 & U_{yy}^0 & 0 \\ 0 & 0 & U_{zz}^0 \end{pmatrix} \tag{11}$$

where U_{xx}^0, U_{yy}^0 and U_{zz}^0 are evaluated at the geostationary point. The sail attitude is fixed such that $\boldsymbol{u}$ points along the Sun-line but is pitched at an angle α only. Substituting $\delta = 0$ in Eq. (8), Eq. (10) can then be written in component form as

$$\frac{d^2\xi}{dt^2} - 2\frac{d\eta}{dt} + U_{xx}^0\xi = a_0\cos^3\alpha\,\cos(\Omega^*t) = a_\xi \tag{12}$$

$$\frac{d^2\eta}{dt^2} + 2\frac{d\xi}{dt} + U_{yy}^0\eta = -a_0\cos^3\alpha\,\sin(\Omega^*t) = a_\eta \tag{13}$$

$$\frac{d^2\zeta}{dt^2} + U_{zz}^0\zeta = a_0\cos^2\alpha\,\sin\alpha = a_\zeta \tag{14}$$

Equations (12-14) define the linearized model for the forced nonlinear system defined by Eq. (4). If the input $\boldsymbol{a} = (a_\xi, a_\eta, a_\zeta)^T$ does not drive the system very far from equilibrium, then the linearized model is a valid representation of Eq. (4), as the system is then operating in the linear range.

The solution for the uncoupled out-of-plane equation of motion Eq. (14) is given by

$$\zeta = \left(\zeta^0 - \frac{a_0\cos^2\alpha\sin\alpha}{U_{zz}^0}\right)\cos(\sqrt{U_{zz}^0}\,t) + \frac{a_0\cos^2\alpha\sin\alpha}{U_{zz}^0} \tag{15}$$

Therefore, the motion along ζ is a periodic oscillation at an out-of-plane equatorial distance $a_0\cos^2\alpha\sin\alpha/U_{zz}^0$. To remove the periodic oscillation, the initial out-of-plane equatorial distance is chosen as

$$\zeta^0 = \frac{a_0\cos^2\alpha\sin\alpha}{U_{zz}^0} = \frac{a_\zeta}{U_{zz}^0} \tag{16}$$

and so the sail then remains at this distance. Eq. (16) shows that for a fixed ζ^0, the gravitational acceleration along the z_e-axis (i.e., $\zeta^0 U_{zz}^0$) must be balanced by two parameters a_0 and the pitch angle α. For fixed ζ^0, the sail characteristic acceleration a_0 can be minimized for an optimal choice of pitch angle determined by

$$\frac{d\cos^2\alpha\sin\alpha}{d\alpha} = 0$$
$$\alpha^* = \tan^{-1}(2^{-1/2})$$
$$\alpha^* = 35.264° \tag{17}$$

The autonomous (unforced) coupled Eqs. (12-13) have an eigenvalue spectrum $(\pm i, 0, 0)$. An in-plane particular solution of Eqs. (12-13) can be assumed that is periodic with the same frequency as the sail forcing Ω^* in the rotating frame, that is

$$\xi = A_\xi\cos(\Omega^*t) + B_\xi\sin(\Omega^*t)$$
$$\eta = A_\eta\cos(\Omega^*t) + B_\eta\sin(\Omega^*t) \tag{18}$$

Substituting Eq. (18) in Eqs. (12-13) and equating the coefficients of $\cos(\Omega^*t)$ and $\sin(\Omega^*t)$, the following linear equations for A_ξ, A_η, B_ξ and B_η are obtained

$$\begin{pmatrix} U_{xx}^0 - \Omega^{*2} & 0 & 0 & -2\Omega^* \\ 0 & 2\Omega^* & U_{xx}^0 - \Omega^{*2} & 0 \\ 0 & -\Omega^{*2} + U_{yy}^0 & 2\Omega^* & 0 \\ -2\Omega^* & 0 & 0 & -\Omega^{*2} + U_{yy}^0 \end{pmatrix}\begin{pmatrix} A_\xi \\ A_\eta \\ B_\xi \\ B_\eta \end{pmatrix} = \begin{pmatrix} a_0\cos^3\alpha \\ 0 \\ 0 \\ -a_0\cos^3\alpha \end{pmatrix} \tag{19}$$

so that the coefficients of the particular solution which define the size of the orbit are given by

$$A_\xi = \frac{\sqrt{a_\xi^2 + a_\eta^2}(U_{yy}^0 - 2\Omega^* - \Omega^{*2})}{\Omega^{*4} - \Omega^{*2}(4 + U_{yy}^0 + U_{xx}^0) + U_{xx}^0 U_{yy}^0} = -551.131a_p$$
$$A_\eta = 0$$
$$B_\xi = 0$$
$$B_\eta = \frac{-A_\xi(\Omega^{*2} + 2\Omega^* - U_{xx}^0)}{(\Omega^{*2} + 2\Omega^* - U_{yy}^0)} = -2.00365A_\xi = 1104.273a_p \tag{20}$$

American Institute of Aeronautics and Astronautics

where $a_p = \sqrt{a_\xi^2 + a_\eta^2} = a_0 \cos^3 \alpha$. Therefore, the solution to Eqs. (12-14) can be written as

$$
\begin{aligned}
\xi(t) &= A_\xi \cos(\Omega^* t) \\
\eta(t) &= B_\eta \sin(\Omega^* t) \\
\zeta(t) &= \zeta^0
\end{aligned}
\tag{21}
$$

The component of the sail acceleration parallel to the equatorial plane $a_p = a_0 \cos^3 \alpha$ determines the
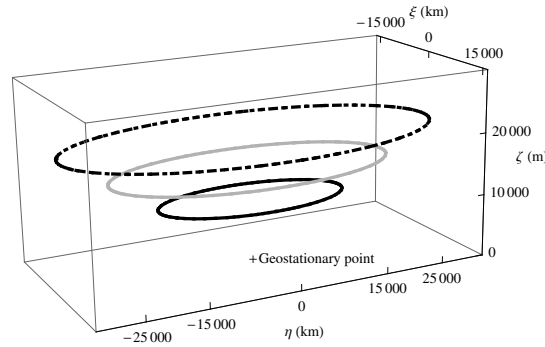

Figure 3. Displaced solar sail orbits of period $T = 2\pi/\Omega^*$ around a geostationary point. The solar sails are pitched at $\alpha^* = 35.264°$ on each orbit. For the solid-line orbit at $\zeta^0 = 0.000237168$ (10 km), the gray-line orbit at $\zeta^0 = 0.000355752$ (15 km) and the dashed-line orbit at $\zeta^0 = 0.000474336$ (20 km), the sails require a characteristic acceleration $a_0^* = 0.000616181$ (0.138 mms^{-2}), $a_0^* = 0.000924272$ (0.207 mms^{-2}) and $a_0^* = 0.00123236$ (0.276 mms^{-2}) respectively.

semi-major and semi-minor axes (A_ξ, B_η) of the elliptic displaced orbit (see Eq. 20) while the component out-of-the-equatorial plane $a_\zeta = a_0 \cos^2 \alpha \sin \alpha$ determines the displacement above the equatorial plane (see Eq. 16).
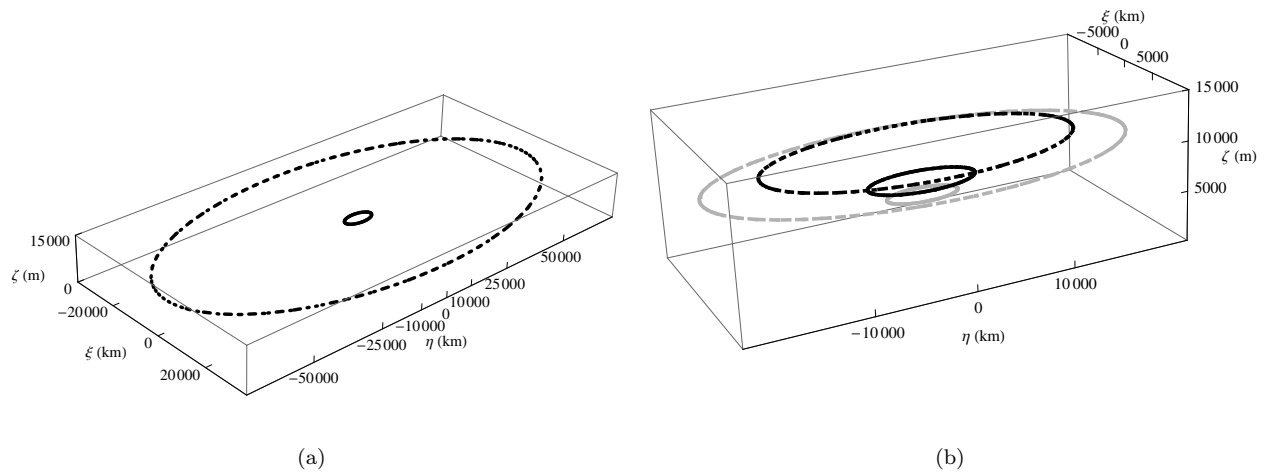

(a)   (b)

Figure 4. Displaced orbits of period $T = 2\pi/\Omega^*$. (a) The two orbits are at the same displacement $\zeta^0 = 0.000237168$ (10 km) for a sail with $a_0 = 0.001561$ (0.35 mms^{-2}). The sail is pitched at angle $\alpha_1 = 8.95°$ for the dashed-line orbit and at an angle $\alpha_2 = 65.92°$ for the solid-line orbit so that $\cos^2 \alpha_1 \sin \alpha_1 = \cos^2 \alpha_2 \sin \alpha_2$ (b) For a sail with a_0 (0.138mms^{-2}), multiple orbits are shown at different displacements ζ^0 by varying the pitch angle at $60°$ (the gray solid-line orbit), $55°$ (the black solid-line orbit), $35.264°$ (the black dashed-line orbit), $25°$ (the gray dashed-line orbit).

Figure 3 shows displaced elliptic orbits at displacement ζ^0 (i.e., along z_e axis) corresponding to 10 km,

15 km, and 20 km. The three sails have a minimum sail characteristic acceleration a_0^* on the displaced orbits corresponding to the optimum sail pitch angle α^*. Figure 3 shows that orbits with large displacements ζ^0 above the Earth equatorial plane need large a_0^*, as expected. However, the size A_ξ, B_η of the displaced orbits also increases as the in-plane sail acceleration a_p increases.

Figure 4a shows that for a sail with characteristic acceleration $a_0 > a_0^*$, for a given ζ^0, then two displaced orbits can be generated corresponding to two specific sail pitch angles. These pitch angles α_1 and α_2 can be determined by solving Eq. (16) numerically. Thus, for a sail with $a_0 > a_0^*$ at a given ζ^0, a displaced orbit is parameterized by a_0 and α. Fig. 4a also shows that for a larger pitch angle α_2, the size A_ξ, B_η of the elliptic displaced orbit decreases due to the decrease of a_p ($a_0 \cos^3 \alpha_2 < a_0 \cos^3 \alpha_1$). Therefore, an orbit with a large pitch angle α_2 does not drive the system far from the geostationary point. Fig. 4b shows for a given sail with a_0 (0.138mms^{-2}), multiple orbits obtained at different ζ^0 by varying the sail pitch angle α. Note that the maximum displacement ζ^0 orbit, for a given a_0, also corresponds to $\alpha = 35.264°$.

IV.   Accommodating the Nonlinearities

The linearized model considered in Eqs. (12-13) is a linear nonautonomous system because the linearized system considers that the Sun-line $\hat{\boldsymbol{S}}(t)$ is changing direction in the rotating frame but neglects the effect of the non-linear Earth gravity. Thus, the displaced orbit of the linear system will not be periodic in the nonlinear system Eq.(4) due to the non-linear gravitational terms. In this section, displaced orbits for the full nonlinear nonautonomous systems will be investigated.

If $\boldsymbol{x}^T = \begin{bmatrix} \boldsymbol{r}^T, \boldsymbol{v}^T \end{bmatrix}$ denotes the state vector then Eq. (4) can be rewritten in rotating frame as

$$\dot{\boldsymbol{x}} = \boldsymbol{f}(t, \boldsymbol{x}, \boldsymbol{u}) = \begin{pmatrix} \boldsymbol{v} \\ -2\boldsymbol{\omega}_e \times \frac{d\boldsymbol{r}}{dt} - \nabla U + \boldsymbol{a}(t, \boldsymbol{u}) \end{pmatrix} \tag{22}$$

The collocation scheme from reference[10] is adapted to find displaced periodic orbits of Eq. (22). However, a pre-defined box around the linear periodic solution Eq. (21) as a path constraint and the complete analytical Jacobian matrix (for faster convergence) are implemented in this paper; these will be discussed in following sections.

A.   Statement of Problem and Minimum Norm Solution

The problem of finding the displaced periodic orbit for the nonlinear nonautonomous system Eq. (22) can be reduced to finding the solution of the (nonlinear) vector constraint. However, the period of the orbit $T = 2\pi/\Omega^*$ is known beforehand since the dynamical system is nonautonomous. The constraints that need to be satisfied for computing the displaced periodic orbits are

- The collocation constraint of the Hermite Simpson method.[21] The time domain ($0 = t_1 < t_2 < \cdots < t_n = T$) is divided into n nodes, and $n-1$ segments whereas the ith segment connects two neighboring nodes at time t_i and t_{i+1}. The differential equations are automatically satisfied at the node points. In general, they will not be satisfied at the mid point of the segment, so the collocation constraint at the segment center $t_{i,c} = (t_i + t_{i+1})/2$ is given by

$$\begin{aligned} \boldsymbol{\Delta}_{i,c}(\boldsymbol{x}_i, \boldsymbol{u}_i, \boldsymbol{x}_{i+1}, \boldsymbol{u}_{i+1}) &= \boldsymbol{x}_{i+1} - \boldsymbol{x}_i - \frac{h}{6}\{\boldsymbol{f}(t_i, \boldsymbol{x}_i, \boldsymbol{u}_i) + 4\boldsymbol{f}(t_{i,c}, \boldsymbol{x}_{i,c}, \boldsymbol{u}_{i,c}) + \boldsymbol{f}(t_{i+1}, \boldsymbol{x}_{i+1}, \boldsymbol{u}_{i+1})\} \\ &= 0 \end{aligned} \tag{23}$$

where $h = t_{i+1} - t_i$, and $\boldsymbol{x}_i, \boldsymbol{x}_{i+1}, \boldsymbol{u}_i$, and $\boldsymbol{u}_{i+1}$ denote the states and controls at node points t_i and t_{i+1} respectively for the ith segment. The mid point control $\boldsymbol{u}_{i,c} = (\boldsymbol{u}_i + \boldsymbol{u}_{i+1})/2$ and state $\boldsymbol{x}_{i,c}$ at the segment centre is given by

$$\boldsymbol{x}_{i,c} = \frac{1}{2}(\boldsymbol{x}_i + \boldsymbol{x}_{i+1}) + \frac{h}{8}\{\boldsymbol{f}(t_i, \boldsymbol{x}_i, \boldsymbol{u}_i) - \boldsymbol{f}(t_{i+1}, \boldsymbol{x}_{i+1}, \boldsymbol{u}_{i+1})\}$$

- Equality constraints that satisfy the definition of the periodic orbit. Therefore, the initial and the end point constraint at t_1 and t_n are

$$\begin{aligned} h_1(x_1, x_n) &= x_n - x_1 = 0, & h_2(y_1, y_n) &= y_n - y_1 = 0, & h_3(z_1, z_n) &= z_n - z_1 = 0, \\ h_4(\dot{x}_1, \dot{x}_n) &= \dot{x}_n - \dot{x}_1 = 0, & h_5(\dot{y}_1, \dot{y}_n) &= \dot{y}_n - \dot{y}_1 = 0, & h_6(\dot{z}_1, \dot{z}_n) &= \dot{z}_n - \dot{z}_1 = 0 \end{aligned} \tag{24}$$

$$h_7(u_1^{(1)}, u_n^{(1)}) = u_n^{(1)} - u_1^{(1)} = 0$$
$$h_8(u_1^{(2)}, u_n^{(2)}) = u_n^{(2)} - u_1^{(2)} = 0 \qquad (25)$$
$$h_9(u_1^{(3)}, u_n^{(3)}) = u_n^{(3)} - u_1^{(3)} = 0$$

where $\boldsymbol{u}_i = (u_i^{(1)}, u_i^{(2)}, u_i^{(3)})^T$

- Equality constraint at point t_i. This control constraint represents the fact that the sail orientation can be controlled by only two angles i.e., sail pitch angle α and yaw angle δ

$$\psi_i(\boldsymbol{u}_i) = \|\boldsymbol{u}_i\|^2 - 1, \quad i = 1, 2, \cdots, n \qquad (26)$$

- The inequality path constraints $\tilde{\boldsymbol{g}}_i(\boldsymbol{x}_i, \boldsymbol{u}_i) < 0$ of the m-element column vector are handled as an equality constraint by using slack variables. The idea is that if $\tilde{g}_i^{(j)}(\boldsymbol{x}_i, \boldsymbol{u}_i) < 0$, then $\tilde{g}_i^{(j)}$ plus some positive number (i.e., slack variable) is equal to zero. To find displaced periodic orbits at a given displacement ζ^0 of the nonlinear system Eq. (22), the path constraint is applied by choosing a box in the neighborhood of the corresponding linearized displaced periodic orbit (see Sec.II). The path constraint forces the solution to remain inside a pre-defined box above the Earth equatorial plane. If $\boldsymbol{r}_{lb} = (x_{lb}, y_{lb}, z_{lb})^T$ and $\boldsymbol{r}_{ub} = (x_{ub}, y_{ub}, z_{ub})^T$ denote the lower and upper bounds of the box, then the inequality path constraint $\tilde{\boldsymbol{g}}_i = \begin{pmatrix} \boldsymbol{r}_{lb} - \boldsymbol{r}_i \\ \boldsymbol{r}_i - \boldsymbol{r}_{ub} \end{pmatrix} < 0$ can be written as

$$\boldsymbol{g}_i(\boldsymbol{r}_i, \boldsymbol{k}_i) = \begin{pmatrix} \boldsymbol{r}_{lb} - \boldsymbol{r}_i \\ \boldsymbol{r}_i - \boldsymbol{r}_{ub} \end{pmatrix} + \boldsymbol{k}_i^2 = 0, \quad i = 1, 2, \cdots, n \qquad (27)$$

where $\boldsymbol{k}_i^2 = [(k_i^{(1)})^2, (k_i^{(2)})^2, \cdots, (k_i^{(m)})^2]^T$ denote the vector i.e., the element-wise square of the m-element slack variable $\boldsymbol{k}_i$ and $m = 6$. The constraints given in Eqs. (23-26) are necessary constraints for computing a periodic orbit for the solar sail. However, these constraint together with the pre-defined box constraint Eq. (27) are necessary to have the NKO above the Earth equatorial plane with the collocation scheme. Newton's method is used to find the solutions of the (nonlinear) algebraic equations $\boldsymbol{C}(\boldsymbol{X}) = 0$ for the root $\boldsymbol{X}^* = 0$.

For this problem, the single vector $\boldsymbol{X}$ is defined including all the independent variables i.e., node states and control, and slack variables. Therefore,

$$\boldsymbol{X}^T = \left[\boldsymbol{x}_1^T, \boldsymbol{u}_1^T, \boldsymbol{x}_2^T, \boldsymbol{u}_2^T, \cdots, \boldsymbol{x}_n^T, \boldsymbol{u}_n^T, \boldsymbol{k}_1^T, \boldsymbol{k}_2^T, \cdots, \boldsymbol{k}_n^T \right] \qquad (28)$$

where n is the total number of nodes. Therefore, the total number of free parameters in $\boldsymbol{X}^T$ is $6n + 3n + nm = n(9 + m)$: $6n$ for the node states, $3n$ for node controls and nm for the slack variables. Secondly, the full constraint vector $\boldsymbol{C}$ consists of defect constraints, path constraints, and specific nodal constraints and is defined as

$$\boldsymbol{C}(\boldsymbol{X})^T = (\boldsymbol{\Delta}_{1,c}^T, \boldsymbol{\Delta}_{2,c}^T, \cdots, \boldsymbol{\Delta}_{n-1,c}^T, \psi_1, \psi_2, \cdots, \psi_n, \boldsymbol{g}_1^T, \boldsymbol{g}_2^T, \cdots, \boldsymbol{g}_n^T, h_1, h_2, \cdots, h_9) = 0 \qquad (29)$$

Therefore a total of $6(n-1) + n + nm + 9 = n(7 + m) + 3$ constraints exist: $6(n-1)$ for the defect, n for the node controls, nm for the path constraints, and 9 for the node constraints. Note that $m = 6$ for the pre-defined box constraints (see Eq. (27)). The linearization of $\boldsymbol{C}(\boldsymbol{X})$ about the point $\boldsymbol{X}_j$ gives

$$\boldsymbol{C}(\boldsymbol{X}_j) = \mathcal{D}\boldsymbol{C}(\boldsymbol{X}_j)(\boldsymbol{X}_j - \boldsymbol{X}_{j+1}) \qquad (30)$$

where the Jacobian $\mathcal{D}\boldsymbol{C} \in \mathbb{R}^{(n(7+m)+3) \times (n(9+m))}$ and $\boldsymbol{C}(\boldsymbol{X}_j) \in \mathbb{R}^{n(7+m)+3}$. The unique solution with minimum norm $\|\boldsymbol{X}_j - \boldsymbol{X}_{j+1}\|$ subjected to Eq. (30) is called the minimum norm solution.[22] Using the pseudoinverse of $\mathcal{D}\boldsymbol{C}(\boldsymbol{X}_j)$, then, $\boldsymbol{X}_{j+1}$ closest to $\boldsymbol{X}_j$ is

$$\boldsymbol{X}_{j+1} = \boldsymbol{X}_j - \mathcal{D}\boldsymbol{C}(\boldsymbol{X}_j)^T \left[\mathcal{D}\boldsymbol{C}(\boldsymbol{X}_j) \cdot \mathcal{D}\boldsymbol{C}(\boldsymbol{X}_j)^T \right]^{-1} \boldsymbol{C}(\boldsymbol{X}_j) \qquad (31)$$

The algorithm converges quadratically until $\|C(X_{j+1})\|$ is satisfied within prescribed tolerance (within 10^{-10}). In Eq. (30), the Jacobian $\mathcal{D}C$ is a very large sparse matrix (see Ozimek et al.[10] for a detailed discussion on calculating $\left[\mathcal{D}C \cdot \mathcal{D}C^T\right]^{-1} C$ that exploits the sparse structure of $\mathcal{D}C$). In this paper, all the non-zero elements $\mathcal{D}\Delta_{i,c}, \mathcal{D}\psi_i, \mathcal{D}g_i$ and $\mathcal{D}h_l$ of the Jacobian $\mathcal{D}C$ are calculated analytically (note that defect derivatives $\mathcal{D}\Delta_{i,c}$ are calculated numerically in Reference 10 because a seventh degree polynomial approximation for the states is used therein rather than the Hermite-Simpson method). The 6×18 defect derivatives matrix $\mathcal{D}\Delta_{i,c}$ is computed as

$$\mathcal{D}\Delta_{i,c} = \left\{ \frac{\partial\Delta_{i,c}}{\partial x_i}, \frac{\partial\Delta_{i,c}}{\partial x_{i+1}}, \frac{\partial\Delta_{i,c}}{\partial u_i}, \frac{\partial\Delta_{i,c}}{\partial u_{i+1}} \right\} \tag{32}$$

The derivatives of the defect vector $\Delta_{i,c}$ with respect to states at the node points of the ith segment are obtained from Eq. (23), and are given by

$$\frac{\partial\Delta_{i,c}}{\partial x_i} = -I_6 - \frac{h}{6}\left[F(t_i, x_i, u_i) + 4F(t_{i,c}, x_{i,c}, u_{i,c})\frac{\partial x_{i,c}}{\partial x_i} \right]$$
$$\frac{\partial\Delta_{i,c}}{\partial x_{i+1}} = I_6 - \frac{h}{6}\left[F(t_{i+1}, x_{i+1}, u_{i+1}) + 4F(t_{i,c}, x_{i,c}, u_{i,c})\frac{\partial x_{i,c}}{\partial x_{i+1}} \right] \tag{33}$$

for $i = 1, 2, \cdots, n-1$, where F denotes the 6×6 matrix, and results from the differentiation of the right side of the Eq.(22) $f(t, x, u)$ with respect to states x. I_6 is the 6×6 identity matrix, and

$$\frac{\partial x_{i,c}}{\partial x_i} = \frac{I_6}{2} + \frac{h}{8}F(t_i, x_i, u_i)$$
$$\frac{\partial x_{i,c}}{\partial x_{i+1}} = \frac{I_6}{2} - \frac{h}{8}F(t_{i+1}, x_{i+1}, u_{i+1}) \tag{34}$$

The derivatives with respect to the controls are found to be

$$\frac{\partial\Delta_{i,c}}{\partial u_i} = -\frac{h}{3}\left[G(t_{i,c}, x_{i,c}, u_{i,c}) + \left\{ \frac{I_6}{2} + \frac{h}{4}F(t_{i,c}, x_{i,c}, u_{i,c}) \right\} G(t_i, x_i, u_i) \right]$$
$$\frac{\partial\Delta_{i,c}}{\partial u_{i+1}} = -\frac{h}{3}\left[G(t_{i,c}, x_{i,c}, u_{i,c}) + \left\{ \frac{I_6}{2} - \frac{h}{4}F(t_{i,c}, x_{i,c}, u_{i,c}) \right\} G(t_{i+1}, x_{i+1}, u_{i+1}) \right] \tag{35}$$

for $i = 1, 2, \cdots, n-1$, where G denotes the 6×3 matrix, and results from differentiation of the right side of equation $f(t, x, u)$ with respect to the control vector u. $\mathcal{D}\psi_i, \mathcal{D}g_i$ and $\mathcal{D}h_l$ are given in the appendix.

B.   Illustrative Examples

In this section periodic orbits will be illustrated for Eq. (22) using the collocation scheme with inequality path constraints i.e., Eq. (27). Again it is assumed that the Sun-line $\hat{S}(t)$ is in the Earth's equatorial plane. The period of the orbit is known ($T = \frac{2\pi}{\Omega^*}$) and is divided into $n = 100$ node points. Once $u_i = (u_i^{(1)}, u_i^{(2)}, u_i^{(3)})$ is known from the converged solution $X^* = X_{j+1}$ of Eq. (31), the sail pitch α_i and δ_i angle can be calculated as

$$\alpha_i = \sin^{-1} u_i^{(3)} \tag{36}$$
$$\delta_i = \tan^{-1}\left(\frac{u_i^{(1)} \sin\Omega^* t_i + u_i^{(2)} \cos\Omega^* t_i}{u_i^{(1)} \cos\Omega^* t_i - u_i^{(2)} \sin\Omega^* t_i} \right) \tag{37}$$

If inequality path constraints are neglected i.e., Eq. (27), then the problem for computing periodic orbits reduces to satisfying the defect constraints, periodic orbit definition constraints and the control constraints $\psi_i = 0$. The collocation scheme initially generates periodic solutions of period $T = \frac{2\pi}{\Omega^*}$, however, it is not a displaced orbit since it crosses the Earth's equatorial plane. Such orbits will not be investigated in this paper. However, this result suggests inequality path constraints must be enforced to investigate displaced periodic orbits of Eq. (22).

A box in the neighborhood of the linearized forced periodic solution Eq. (21) is chosen as an inequality path constraint (see Eq. (27)). The lower and upper bounds of the the box i.e., $\boldsymbol{r}_{lb} = (x_{lb}, y_{lb}, z_{lb})^T$ and $\boldsymbol{r}_{ub} = (x_{ub}, y_{ub}, z_{ub})^T$ are defined as

$$
\begin{aligned}
x_{lb} &= 1 + \xi_{min} + \nu\xi_{min}, & x_{ub} &= 1 + \xi_{max} + \nu\xi_{max} \\
y_{lb} &= \eta_{min} + \nu\eta_{min}, & y_{ub} &= \eta_{max} + \nu\eta_{max} \\
z_{lb} &= \zeta^0 - \mu\zeta^0, & z_{ub} &= \zeta^0 + \mu\zeta^0
\end{aligned}
\tag{38}
$$

where $\xi_{min} < 0$, $\xi_{max} > 0$, $\eta_{min} < 0$ and $\eta_{max} > 0$ are the minimum and maximum x and y position on the linearized periodic displaced periodic orbit from the geostationary point. $\zeta^0 > 0$ is the desired displacement above the Earth's equatorial plane and ν and μ are parameters used for sizing the box dimensions.
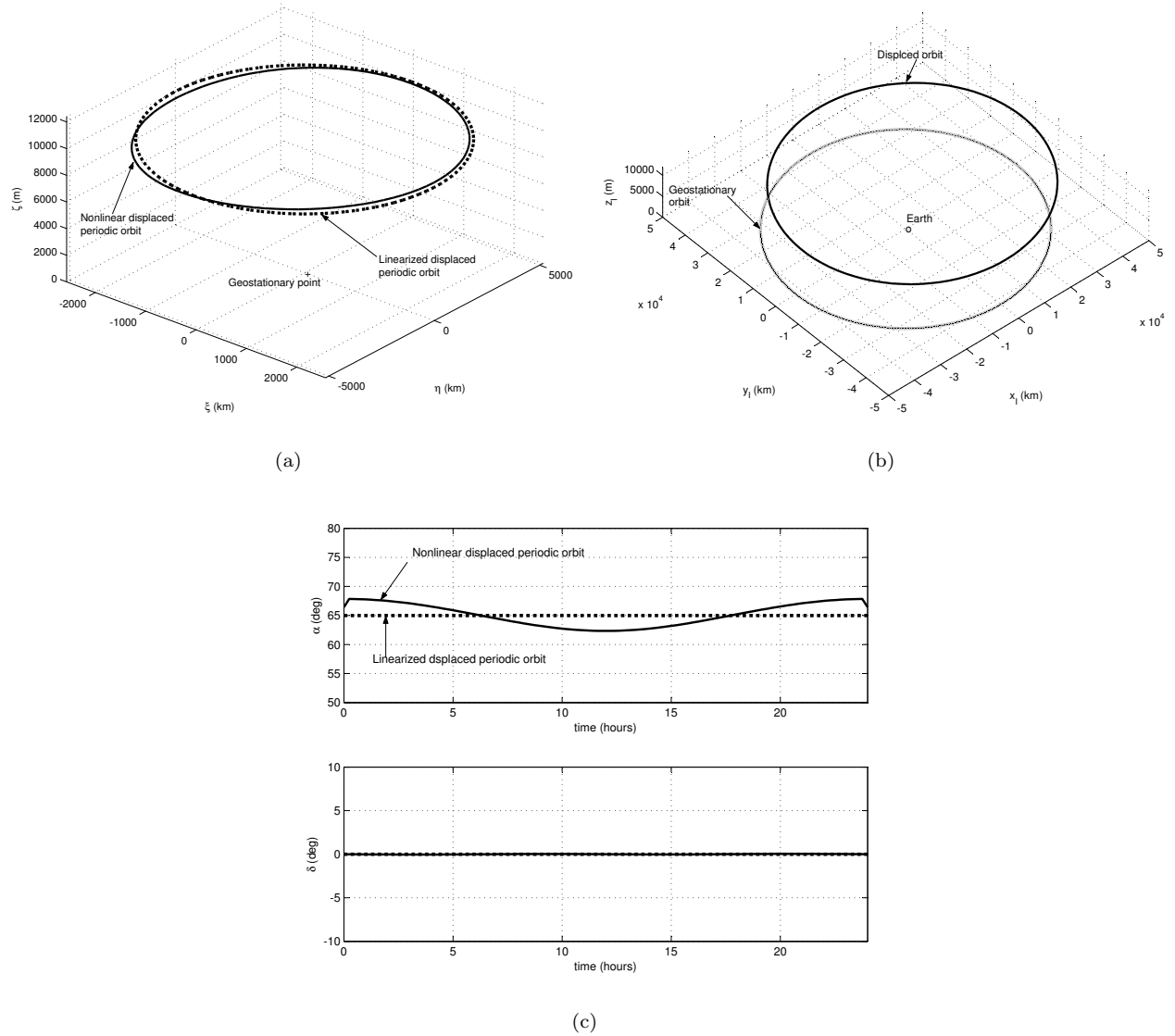

(a)

(b)

(c)

Figure 5. A sail with characteristic acceleration 0.328 mms^{-2} **shows a displaced periodic orbit of period** $T = \frac{2\pi}{\Omega^*}$ **around a geostationary point (a) in the ECEF frame (b) in the ECI frame (the black solid line orbit is a non-Keplerian orbit from the collocation scheme and the gray solid line orbit is the Keplerian geostationary orbit) and (c) control history.**

The sail characteristic acceleration is chosen as $a_0 > a_0^*$ for a given ζ^0 to force the spacecraft in a region above the Earth's equatorial plane. A nearby solution will only exist if the chosen sail characteristic acceleration is sufficient to overcome the non-linearities of the gravitational acceleration near the geostationary

American Institute of Aeronautics and Astronautics

point. To compute a displaced periodic orbit at 10 km above the Earth's equatorial plane, a sail characteristic acceleration of 0.328 mms^{-2} is required with the corresponding pitch angle $\alpha = 65°$ determined from Eq. (16). A value of $\alpha > \alpha^*$ is required to avoid a large ellipse (see Fig. 4a). The vector $\boldsymbol{X}$ is given by Eq. (28). For the initial guess vector $\boldsymbol{X}$, the initial states $\boldsymbol{x}_i$ at all node points are the linearized solution, and the initial guess for $\boldsymbol{u}_i$ is computed from Eq. (8) with $t = t_i$, $\delta(t_i) = 0$ and $\alpha(t_i) = 65°$. The initial guess at all node points for slack variables can be determined by solving Eq. (27) for k_i. For $n = 100$ node points, the size of $\boldsymbol{X}$ and $\boldsymbol{C}$ are 1500 and 1303 respectively. Some 99.45% of entries in the matrix $\mathcal{D}\boldsymbol{C}$ are zero because of the sparse structure $\mathcal{D}\boldsymbol{C}$. With a few iterations of Eq. (31), the collocation scheme finds the displaced periodic orbit satisfying the constraints Eqs. (23-26) and path constraint Eq. (27). $\nu = 0.25$ and $\mu = 0.15$ are chosen in the simulation. The resulting displaced orbit is shown by the solid-line in Fig. 5(a). The required sail pitch α and yaw δ angles are also shown by the solid-line in Fig. 5c. The pitch angle is smooth and slowly varying except at the end points (where only a few degrees per hour slew rate is required). Although the control angle rates are not constrained, they can be easily included in the collocation scheme. No variation of the sail yaw δ is seen which suggests that the algorithm averages out the gravitational acceleration along the z axis to generate the displaced periodic orbit 10 km above the Earth equatorial plane. Fig. 5a shows the displaced periodic orbits in the ECEF frame. The displaced periodic orbits computed from the collocation scheme can then be transformed into ECI frame using

$$\begin{pmatrix} x_I \\ y_I \\ z_I \end{pmatrix} = C_{i/e} \begin{pmatrix} x \\ y \\ z \end{pmatrix} \tag{39}$$

Since the Earth angular velocity w_e is unity in non-dimensional units, a rotation matrix $C_{i/e}$ from ECEF to ECI frame is given by

$$C_{i/e} = \begin{pmatrix} \cos t & -\sin t & 0 \\ \sin t & \cos t & 0 \\ 0 & 0 & 1 \end{pmatrix} \tag{40}$$

The displaced periodic orbit is centered around the Earth in the ECI frame and is shown in Fig. 5b. Note that the orbit is non-Keplerian as it does not pass through the center of the Earth. Furthermore, the non-Keplerian orbit is pushed slightly away from the Sun by the solar radiation pressure. Such an offset was also suggested by Forward.[14]

The possibility of displaced periodic orbits for a high performance solar sail is now investigated with a characteristic acceleration of order 6 mms^{-2}.[13] A linearized displaced periodic orbit at $\zeta^0 = 0.0017788$ (about 75 km) with a sail characteristic acceleration $a_0 = 0.0268$ (about 6 mms^{-2}) is chosen as an initial guess for the collocation scheme (see dashed-line orbit and dashed-line control history in Figs. 6a and 6c). The large pitch angle $\alpha = 74.8°$ in the control history is due to $a_0 > a_0^*$ for a given ζ^0 (75 km). This large pitch angle reduces the size A_ξ, B_η of the elliptic displaced orbit around the geostationary point (see Sec. III). $\nu = 0.25$ and $\mu = 0.2$ are chosen for the box dimensions. The collocation scheme converges on a solution which is effectively a 62 km displaced periodic orbit with a control time history shown as the solid-line in Fig. 6. Fig. 6b shows the offset between the displaced orbit and geostationary orbit increases at higher displacements ζ^0. A 75×75 km station-keeping box (i.e., $\pm 0.05°$ in longitude and latitude)[15] around a nominal geostationary point has an upper box-face at 37.5 km above the Earth's equatorial plane, so a 62 km displaced orbit is well above the conventional station-keeping box.

V.   Linear Analysis with Seasonal Effects

So far, it is assumed that the Sun-line is in the Earth's equatorial plane. In reality, depending on the season, the Sun-line moves above and below the Earth's equatorial plane.[16,23] During the summer solstice (June 21) , the Sun-line is 23.5° below the Earth's equatorial plane. During the winter solstice (22 December), the Sun-line is 23.5° above the Earth's equatorial plane. It is only during the equinoxes (March 21, September 23) that the Sun-line is in the Earth's equatorial plane. In this section, a general expression for the forcing term in the linearized model (see Eqs. (12-14)) will be developed i.e., solar sail acceleration (a_ξ, a_η, a_ζ) in ECEF frame valid at the solstices and equinoxes. Secondly, the forcing term is used to analyze the linear model at the solstices.
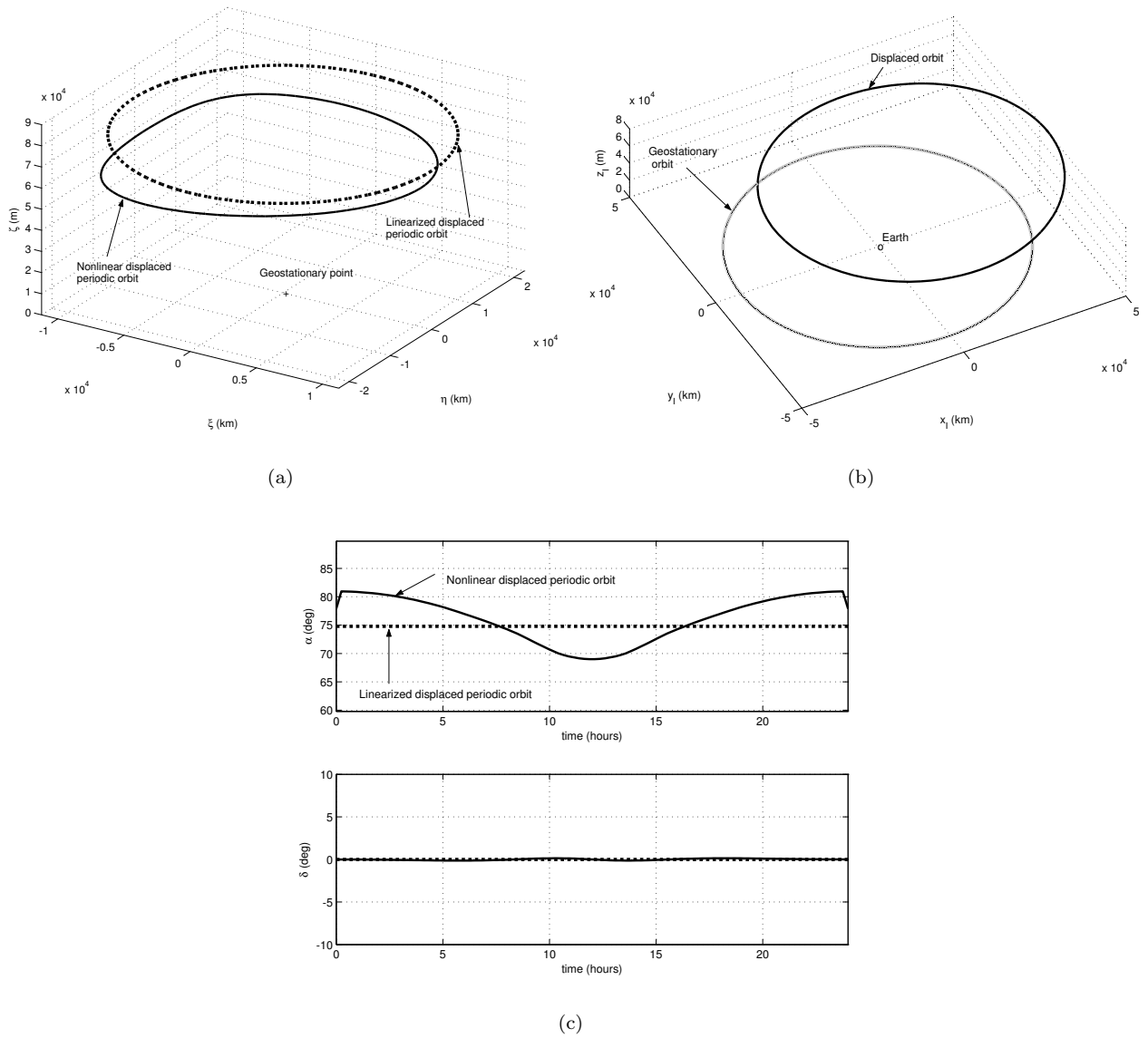
(a)

(b)

(c)

Figure 6. Displaced periodic orbit using a high performance sail with a characteristic acceleration of 6 mms^{-2} (a) in the ECEF frame (b) in the ECI frame and (c) the control history.

A.   Direction of the Sun-line

Fig. 7 shows that the Sun-line $\hat{\boldsymbol{S}}(t)$ is at an angle ϕ above the Earth's equatorial plane. Although ϕ changes
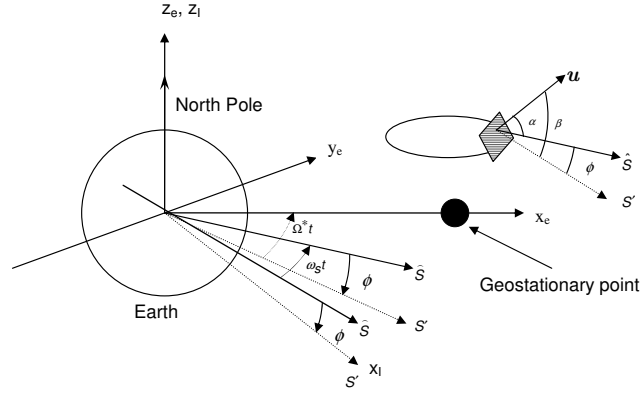

Figure 7.   The Sun-line $\hat{\boldsymbol{S}}$ is shown at an arbitrary angle ϕ above the Earth's equatorial plane. S' is the projection of the Sun-line in the Earth's equatorial plane. The angle $\Omega^* t$ is in the Earth's equatorial plane and the angle ϕ is out of the Earth's equatorial plane. If the angle ϕ is assumed constant over one orbit period, then the Sun-line will move parallel to Earth's equatorial plane, and the angle between projections of the Sun-line in the equatorial plane is also equal to $w_s t$.

with time, it may be assumed fixed for one orbit period T. This is a reasonable assumption given the seperation of time scales (1 day $<<$ 1 year). Now re-define the ECI-frame after each period T (since x_e and $\boldsymbol{S}'$ coincide after one period $T = 2\pi/\Omega^*$) with the x_I-axis now along the projection of the Sun-line $\hat{\boldsymbol{S}}$ in the equatorial plane i.e., along $\boldsymbol{S}'$ (see Fig. 7, x_I and $\boldsymbol{S}'$ coincide at $t = 0$ so that time starts from zero for each simulation run). Then, the direction of the Sun-line $\hat{\boldsymbol{S}}(t)$ and hence the sail normal $\boldsymbol{u}$ in the ECEF-frame are given by

$$\hat{\boldsymbol{S}} = \begin{pmatrix} \cos(\Omega^* t) & \sin(\Omega^* t) & 0 \\ -\sin(\Omega^* t) & \cos(\Omega^* t) & 0 \\ 0 & 0 & 1 \end{pmatrix} \begin{pmatrix} \cos\phi & 0 & -\sin\phi \\ 0 & 1 & 0 \\ \sin\phi & 0 & \cos\phi \end{pmatrix} \begin{pmatrix} 1 \\ 0 \\ 0 \end{pmatrix} = \begin{pmatrix} \cos(\Omega^* t)\cos\phi \\ -\sin(\Omega^* t)\cos\phi \\ \sin\phi \end{pmatrix} \quad (41)$$

$$\boldsymbol{u} = \begin{pmatrix} \cos\beta\cos(\Omega^* t) \\ -\cos\beta\sin(\Omega^* t) \\ \sin\beta \end{pmatrix} \quad (42)$$

Note that in Eq.(6), the angle ϕ is constant and equal to zero over the orbit period T. The angle that the sail normal makes with the Earth's equatorial plane is equal to $\beta(= \alpha + \phi)$. It can be shown that $\hat{\boldsymbol{S}}(t).\boldsymbol{u} = \cos\alpha$.

The Sun-line direction $\hat{\boldsymbol{S}}(t)$ at the autumn/spring equinoxes, the winter and the summer solstices is obtained by substituting $\phi = 0$, $\phi = +\phi_m = +23.5°$ and $\phi = -\phi_m = -23.5°$ respectively in the Eq. (41).

B.   Linearized Solution

In summary, the forcing term of the linearized model i.e., $\boldsymbol{a}$ given on the right-side of Eqs. (12-14)), in the ECEF-frame may be written as

$$\begin{pmatrix} a_\xi \\ a_\eta \\ a_\zeta \end{pmatrix} = a_0 \cos^2\alpha \begin{pmatrix} \cos\beta\cos(\Omega^* t) \\ -\cos\beta\sin(\Omega^* t) \\ \sin\beta \end{pmatrix} \quad (43)$$

where β is given by

$$\begin{aligned} \beta &= \alpha & \text{at autumn/spring equinoxes} \\ \beta &= \alpha - \phi_m & \text{at summer solstice} \\ \beta &= \alpha + \phi_m & \text{at winter solstice} \end{aligned} \quad (44)$$

American Institute of Aeronautics and Astronautics

Therefore, the angle β is equal to α at the equinoxes and exactly 23.5° less or greater at the solstices. With the sail forcing term defined by Eq. (43), the solution of the linearized Eqs. (12-14) will still have the same form as Eq. (21) except that A_ξ, B_η and ζ^0 are now replaced by

$$A_\xi = \frac{a_0 \cos^2 \alpha \cos \beta \, (U_{yy}^0 - 2\Omega^* - \Omega^{*2})}{\Omega^{*4} - \Omega^{*2}(4 + U_{yy}^0 + U_{xx}^0) + U_{xx}^0 U_{yy}^0} \tag{45}$$

$$B_\eta = \frac{-A_\xi(\Omega^{*2} + 2\Omega^* - U_{xx}^0)}{(\Omega^{*2} + 2\Omega^* - U_{yy}^0)} \tag{46}$$

$$\zeta^0 = \frac{a_0 \cos^2 \alpha \sin \beta}{U_{zz}^0} \tag{47}$$

where β is defined by Eq. (44). The sail acceleration component in the equatorial plane $a_p = \sqrt{a_\xi^2 + a_\eta^2} = a_0 \cos^2 \alpha \cos \beta$ determines the size (A_ξ, B_η) of the elliptic displaced orbit, while the component out-of-the equatorial plane $a_\zeta = a_0 \cos^2 \alpha \sin \beta$ determines the levitation height ζ^0 of the displaced orbit. To size the sail for a mission based on a displaced orbit around a geostationary point, the worst-case scenario should be considered which is the summer solstice (the lowest value of a_ζ in Eq. (43)). Therefore, for a given ζ^0, a_0 could be minimized from the above equation by maximizing $\cos^2 \alpha \sin(\alpha - \phi_m)$, since $\beta = \alpha - \phi_m$ at summer solstice. Therefore,
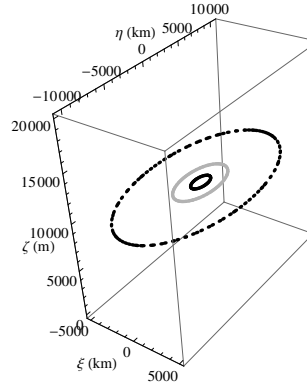

Figure 8. 10 km levitated displaced periodic orbits for a sail with characteristic acceleration $a_0 = 0.002795$ (0.626 mms^{-2}) at summer solstice (dashed-line orbit with $\alpha = 70°$), winter solstice (solid-line black orbit with $\alpha = 73°$) and at autumn/spring equinoxes (gray orbit with $\alpha = 72.65°$).

$$\frac{d \cos^2 \alpha \sin(\alpha - \phi_m)}{d\alpha} = 0$$

$$\tilde{\alpha} = \frac{1}{2}\left[\cos^{-1}\left(\frac{1}{3}\cos \phi_m\right) + \phi_m\right]$$

$$\tilde{\alpha} = 47.850° \tag{48}$$

Denote $\tilde{a}_0$ as the sail characteristic acceleration determined from Eq. (47) corresponding to $\alpha = \tilde{\alpha}$ and $\beta = \tilde{\alpha} - \phi_m$ at a given displacement ζ^0. Now, in order to compensate for the Earth's non-linear gravity with the collocation scheme, the sail characteristic acceleration is chosen as $a_0 > \tilde{a}_0$. Similar to Sect. III, there will be two specific pitch angles α_1 and α_2 for each $a_0 > \tilde{a}_0$. In Fig. 8 the outer most dashed-line shows the linearized periodic orbit at displacement ζ^0 (10 km) with a_0 (0.626 mms^{-2}) $> \tilde{a}_0$(0.286 mms^{-2})) and a sail pitch angle $\alpha = 70°$ determined from Eq. (47) with $\beta = \alpha - \phi_m$ (the worst-case summer solstice). Depending on the season the sun-line angle ϕ will vary. Therefore, for the same sail acceleration and to keep fixed ζ^0 (10 km), the sail pitch angle must vary from $\alpha = 72.6532°$ to $\alpha = 73.008°$ at the equinoxes and winter solstice respectively to form the new linearized displaced periodic orbit. These orbits will act as an initial guess for the collocation scheme to generate the new reference displaced periodic orbits with seasonal effects.

American Institute of Aeronautics and Astronautics

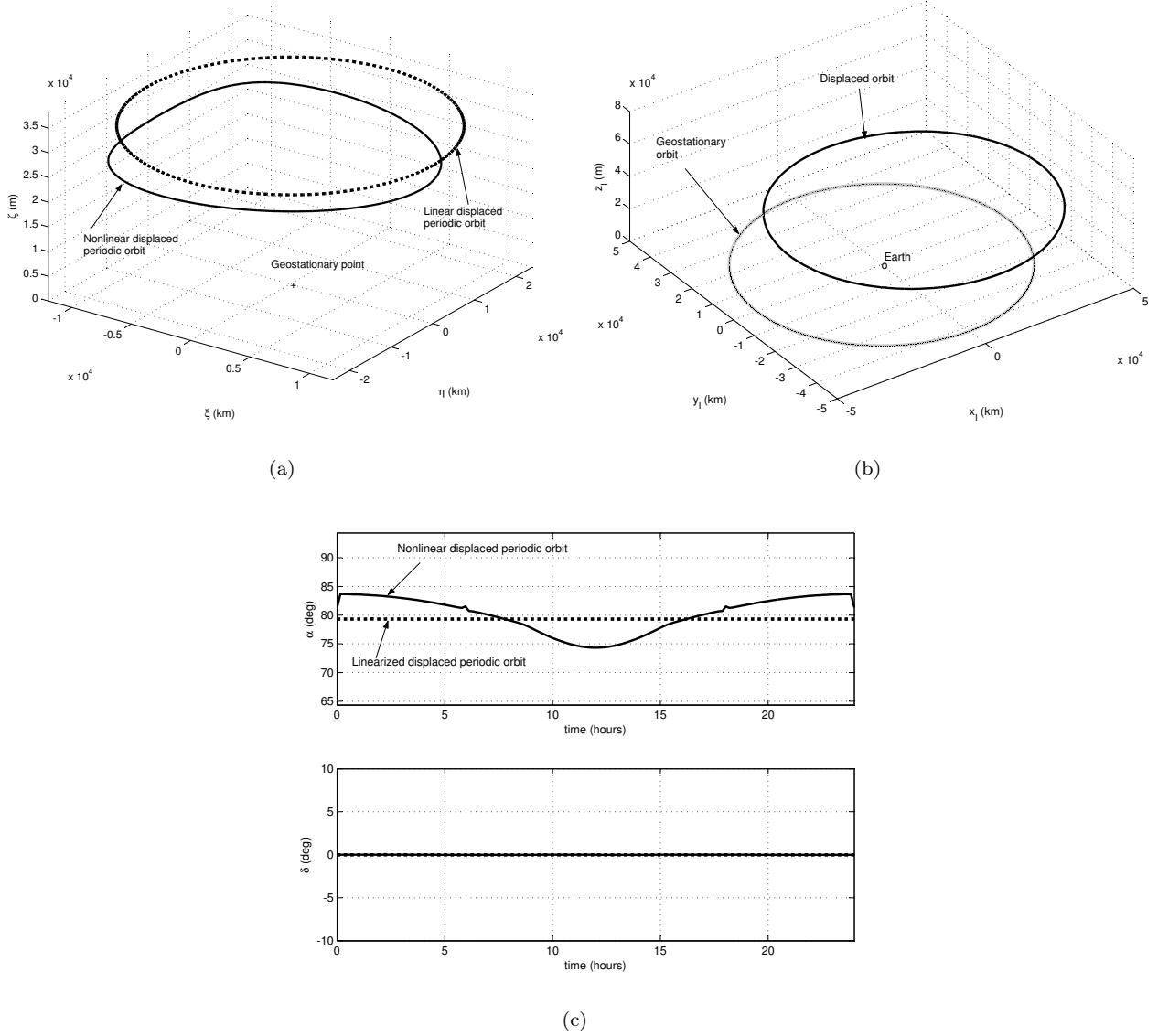# VI.   Illustrative Example at Summer Solstice

(a)

(b)

(c)

Figure 9.   At the summer solstice (worst-case scenario), the displaced periodic orbits for a sail with a characteristic acceleration 6 mms^{-2} (a) in the ECEF frame (b) in the ECI frame and (c) the control history (right).

In this section, the periodic orbits from the collocation scheme are computed for the configuration at the summer solstice with the worst-case geometry. For a displacement ζ^0 (32 km), the collocation scheme converges if the linearized periodic orbit is chosen with a sail characteristic acceleration a_0 (6 mms^{-2}) $> \tilde{a}_0$ (0.916 mms^{-2}), where $\tilde{a}_0$ is computed from $\tilde{\alpha}$ at ζ^0 (32 km). In the linearized solution (see dashed-line in Fig. 9) for a_0 (6 mms^{-2}), the sail pitch angle $\alpha = 79.33°$ is determined from Eq. (47) for $\beta = \alpha - \phi_m$ (summer solstice). In the collocation scheme for the initial guess of the vector $\boldsymbol{X}$, the $\boldsymbol{x}_i$ at all node points ($n = 150$ node points) are from the linearized solution and the initial guess for the components $\mathbf{u}_i$ is computed with $\delta = 0$ and $\alpha = 79.33°$ i.e.,

$$\boldsymbol{u}_i = \begin{pmatrix} \cos(\alpha - \phi_m)\cos(\Omega^* t_i - \delta) \\ -\cos(\alpha - \phi_m)\sin(\Omega^* t_i - \delta) \\ \sin(\alpha - \phi_m) \end{pmatrix} \qquad (49)$$

American Institute of Aeronautics and Astronautics

$\nu = 0.25$ and $\mu = 0.19$ are chosen for sizing the box in Eq. (38) around the linearized solution, and the inequality path constraints Eq. (27) are imposed in the collocation scheme. In Eq. (22), the expression for the Sun-line $\hat{S}$ at the summer solstice (i.e., Eq. (41) with $\phi = -\phi_m$) is used to compute $\boldsymbol{a}$. Therefore, $\boldsymbol{G}$ in Eq. (35) should be modified accordingly in this simulation. The size of $\boldsymbol{X}$ and $\boldsymbol{C}$ are 1953 and 2250 respectively, and some 99.60% of the entries in the matrix $\mathcal{D}\boldsymbol{C}$ are zero. The collocation scheme converges to a periodic solution, a 25 km displaced periodic orbit with control time history shown in Fig. 9 as a solid-line. From $\boldsymbol{X^*}$, the angles δ_i are still calculated from Eq. (37), but the pitch angle α_i is calculated as

$$\alpha_i = \cos^{-1}\left(\frac{u_i^{(1)}}{\cos(\Omega^* t_i - \delta_i)}\right) + \phi_m \qquad (50)$$

The Fig. 9 shows that the collocation scheme finds a periodic orbit displaced 25 km above the Earth's equatorial plane around a geostationary point with a high performance sail. It is noted that for a realistic sail model the large sail pitch angle will result in significant deviation from an ideal solar sail. With the low and moderate performance sail characteristic acceleration such as 0.9 mms^{-2} and 2.15 mms^{-2}, the displaced periodic orbits at the summer solstice with the collocation scheme are found at displacements of 9.5 km and 16 km respectively. However, a sail with a characteristic acceleration of 60 mms^{-2} (a perforated sail[13]), the collocation scheme converges to a displaced periodic orbit at 37.5 km, which is just above the conventional station-keeping box.

These displaced geostationary orbits are unstable as control is required to generate such NKO. The Monodromy matrix $\Phi(t_n, t_1)$ can be calculated as

$$\Phi(t_n, t_1) = \Phi(t_n, t_{n-1}).\Phi(t_{n-1}, t_{n-2}) \cdots \Phi(t_3, t_2).\Phi(t_2, t_1)$$

where $\Phi(t_{i+1}, t_i) = -\left[\frac{\partial \boldsymbol{\Delta}_{i,c}}{\partial \boldsymbol{x}_{i+1}}\right]^{-1}\left[\frac{\partial \boldsymbol{\Delta}_{i,c}}{\partial \boldsymbol{x}_i}\right]$ is calculated from the Jacobian $\mathcal{D}\boldsymbol{C}$ at the converged solution. All six eigenvalues of the Monodromy matrix lie on the unit circle. At the equinoxes for a few weeks, the sail will experience occultation from the Earth's shadow (70 minutes over one orbit period) and it will drop by 4.6% of its initial levitation distance towards the Earth's equatorial plane[16] due to the loss of sail vertical acceleration. Furthermore, the in-plane sail thrust loss during eclipse will deviate it from the NKO. However, these solar sail thrust losses can be compensated for by varying the sail pitch/yaw angle before and after the shadow period. Some other practical issues that need to be addressed are station-keeping requirements and how to achieve precise attitude control on these orbits. For a given sail and levitation distance a full one year simulation can track these nonlinear orbits (if generated on a one day basis (period $2\pi/\Omega^*$) with a fixed Sun declination angle for each day) or to generate bounded motion using the collocation scheme if the initial guess is provided from the one day collocation orbits described in this paper.

VII. Application: Solar Power Transmission from Space

This section describes an example application of light levitated geostationary orbits at $\zeta^0 = \pm 2$ km for reflectors (solar sails pitched at $\alpha = \pm 45°$) of a solar power satellite (SPS) system.[20] The two sails are in formation with a microwave energy generator-transmitter which is orbiting around a geostationary point in the Earth's equatorial plane (i.e., $\zeta^0 = 0$) as shown in Fig. 10a. Note that the energy generator-transmitter has the same in-plane acceleration a_p as the two displaced orbits in-plane acceleration $a_p = a_0 \cos^3 \alpha$ to ensure that the energy generator-transmitter will always be below/above the pitched sails. The orbits of the SPS system illustrated in Fig. 10a are different from reference 20 as the Sun-pointing reflectors and the Earth-pointing transmitter are in orbits around a geostationary point in the ECEF-frame (not stationary in the ECEF-frame). The Sun-light reflected from the levitated sails will fall perpendicularly to the microwave generator-transmitter which will transmit energy to the Earth-receiving antenna.

The dashed-line orbits and the solid-line orbits, shown in Fig. 10b, are generated from the linear analysis and the collocation scheme respectively. The corresponding sail pitch angle α on these orbits is shown in Fig. 10c. The results from the collocation scheme suggests that the sunlight from the sails on displaced orbits will fall almost perpendicularly on the generator-transmitter (offset angle within $\pm 5°$ in Fig. 10c).
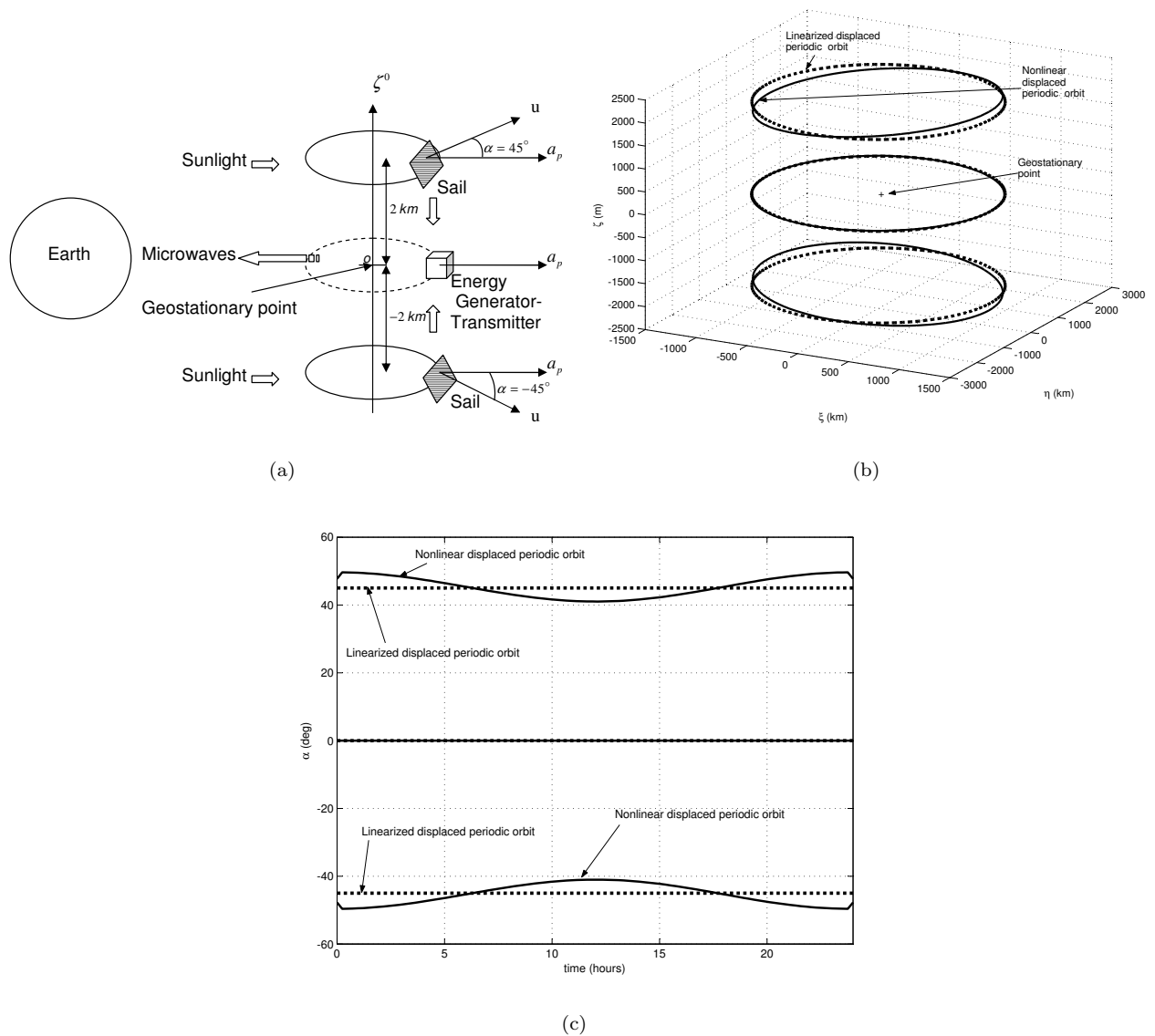
(a)

(b)

(c)

Figure 10. (a) The two solar sails are pitched at $\alpha = \pm 45^\circ$ on displaced orbits (the solid-line orbits) at levitation distance $\zeta^0 = \pm 2$ km. The microwave energy generator-transmitter is orbiting (the dashed-line orbit) in the Earth's equatorial plane and is placed in centre of the system. All three orbits have the same period $T = 2\pi/\Omega^*$ and in-plane acceleration a_p (b) orbits from the linear analysis (sails on displaced orbits with a_0 (0.03 mms^{-2}) (i.e., a_p (0.010635 mms^{-2}) on all orbits)) and the non-linear analysis illustrating the SPS concept in ECEF-frame at the equinoxes (c) sail pitch angle history.

American Institute of Aeronautics and Astronautics

VIII. Conclusions

The possibility of generating displaced non-Keplerian periodic orbits around geostationary points in the solar-sail two body problem has been analyzed. It has been shown that a family of displaced non-Keplerian orbits exist at linear order around the geostationary point. It has also been demonstrated that the collocation scheme is a promising approach to obtain displaced periodic orbits at non-linear order for this problem as the inequality path constraints can be enforced easily. The collocation scheme converges to a periodic solution provided the sail characteristic acceleration is large enough to counter the variation in the Earth's gravity on the displaced orbit around the geostationary point. For a high performance sail with a characteristic acceleration of order 6 mms^{-2} and assuming the Sun-line is in the Earth's equatorial plane, a 62 km non-linear displaced orbit is obtained above the Earth's equatorial plane which is well above the station-keeping box of order 75×75 km of geostationary communication satellites. For the realistic worst-case scenario at the summer solstice, a high performance sail shows a nonlinear displaced periodic orbit at 25 km above the Earth's equatorial plane, while a perforated sail is just above the station-keeping box. Displaced orbits at ± 2 km are illustrated for an application to solar space power generation. These results show that the concept for displaced geostationary orbit reported in the literature is correct, although displacement distances are modest.

Acknowledgments

Appendix: Jacobian Matrix

The elements of $\mathcal{D}\boldsymbol{g}_i$ in the Jacobian matrix $\mathcal{D}\boldsymbol{C}$ are given by

$$\left\{ \frac{\partial \boldsymbol{g}_i}{\partial \boldsymbol{x}_i}, \frac{\partial \boldsymbol{g}_i}{\partial \boldsymbol{u}_i}, \frac{\partial \boldsymbol{g}_i}{\partial \boldsymbol{k}_i} \right\} \tag{51}$$

for $i = 1, 2, \cdots, n$, and

$$\frac{\partial \boldsymbol{g}_i}{\partial \boldsymbol{x}_i} = \begin{pmatrix} -I_3 & O_3 \\ I_3 & O_3 \end{pmatrix}$$

where I_3 and O_3 are the 3×3 identity and null matrix, and

$$\frac{\partial \boldsymbol{g}_i}{\partial \boldsymbol{u}_i} = O_{6 \times 3}, \qquad \frac{\partial \boldsymbol{g}_i}{\partial \boldsymbol{k}_i} = 2\boldsymbol{k}_i^D$$

where $\boldsymbol{k}_i^D$ is the 6×6 diagonal matrix with entries $k_i^{(1)}, k_i^{(2)}, \cdots, k_i^{(6)}$. The non-zero elements in $\mathcal{D}\psi_i$ are $\frac{\partial \psi_i}{\partial \boldsymbol{u}_i} = 2\boldsymbol{u}_i^T$ for $i = 1, 2, \cdots, n$. The non-zero elements of $\mathcal{D}h_l$ are given by

$$\begin{pmatrix} \frac{\partial h_1}{\partial \boldsymbol{x}_1} \\ \frac{\partial h_2}{\partial \boldsymbol{x}_1} \\ \frac{\partial h_3}{\partial \boldsymbol{x}_1} \\ \frac{\partial h_4}{\partial \boldsymbol{x}_1} \\ \frac{\partial h_5}{\partial \boldsymbol{x}_1} \\ \frac{\partial h_6}{\partial \boldsymbol{x}_1} \end{pmatrix} = -I_6, \qquad \begin{pmatrix} \frac{\partial h_1}{\partial \boldsymbol{x}_n} \\ \frac{\partial h_2}{\partial \boldsymbol{x}_n} \\ \frac{\partial h_3}{\partial \boldsymbol{x}_n} \\ \frac{\partial h_4}{\partial \boldsymbol{x}_n} \\ \frac{\partial h_5}{\partial \boldsymbol{x}_n} \\ \frac{\partial h_6}{\partial \boldsymbol{x}_n} \end{pmatrix} = I_6$$

and

$$\begin{pmatrix} \frac{\partial h_7}{\partial \boldsymbol{u}_1} \\ \frac{\partial h_8}{\partial \boldsymbol{u}_1} \\ \frac{\partial h_9}{\partial \boldsymbol{u}_1} \end{pmatrix} = -I_3, \qquad \begin{pmatrix} \frac{\partial h_7}{\partial \boldsymbol{u}_n} \\ \frac{\partial h_8}{\partial \boldsymbol{u}_n} \\ \frac{\partial h_9}{\partial \boldsymbol{u}_n} \end{pmatrix} = I_3$$

American Institute of Aeronautics and Astronautics

References

[1]Heaton, A. F., "Solar Sail Roadmap Mission GNC Challenges," *AIAA Guidance, Navigation, and Control Conference and Exhibit, San Franciso, California, AIAA-2005-6170*, Aug 15-18, 2005.

[2]C. R. McInnes, M. Macdonald, V. A. and Alexander, D., "Geosail: Exploring the Geomagnetic Tail Using a Small Solar Sail," *Journal of Spacecraft and Rockets*, Vol. 38, No. 4, August 2001, pp. 622–629.

[3]M. Macdonald, C. R. McInnes, D. A. and Sandman, A., "Geosail: Exploring the magnetosphere Using a Low-cost Solar Sail," *Acta Astronautica*, Vol. 59, 2006, pp. 757–767.

[4]Macdonald, M., Hughes, G. W., McInnes, C., Lyngvi, A., Falkner, P., and Atzei, A., "GeoSail: An Elegant Solar Sail Demonstration Mission," *Journal of Spacecraft and Rockets*, Vol. 44, No. 4, July-August, 2007, pp. 784–796.

[5]Forward, R., "Statite: a spacecraft that does not orbit," *Journal of Spacecraft and Rockets*, Vol. 28, No. 5, 1991, pp. 606–611.

[6]McInnes, C., McDonald, A., Simmons, J., and McDonald, E., "Solar sail parking in restricted three-body systems," *Journal of Guidance, Control and Dynamics*, Vol. 17, No. 2, 1994, pp. 399–406.

[7]McInnes, C. R., *Solar sailing: technology, dynamics and mission applications*, Springer Praxis, London, 1999, pp.250-256.

[8]McInnes, C. R., "Solar sail Trajectories at the Lunar L_2 Lagrange Point," *Journal of Spacecraft and Rockets*, Vol. 30, No. 6, 1993, pp. 782–784.

[9]Simo, J. and McInnes, C. R., "Solar sail Orbits at the Earth-Moon Libration Points," *Communications in Nonlinear Science and Numerical Simulation*, Vol. 14, No. 12, December 2009, pp. 4191–4196.

[10]M.T. Ozimek, D. G. and Howell, K., "Solar Sails and Lunar South Pole Coverage," *AIAA/AAS Astrodynamics Specialist Conference and Exhibit, Honolulu, Hawaii*, August, 2008.

[11]McInnes, C. R. and Simmons, J. F. L., "Halo Orbits for Solar Sails I-Heliocentric Case," *Journal of Spacecraft and Rockets*, Vol. 29, No. 4, 1992, pp. 466–471.

[12]McInnes, C. R. and Simmons, J. F. L., "Halo Orbits for Solar Sails II-Geocentric Case," *Journal of Spacecraft and Rockets*, Vol. 29, No. 4, 1992, pp. 472–479.

[13]McInnes, C. R., "Solar Sail Mission Applications for Non-keplerian Orbits," *Acta Astronautica*, Vol. 45, No. 4-9, 1999, pp. 567–575.

[14]Forward, R. L., "Light-Levitated Geostationary Cylinderical Orbits Using Perforated Light Sails," *The Journal of Astronautical Sciences*, Vol. 32, No. 2, April-June 1984, pp. 221–226.

[15]Maral, G. and Bousquet, M., *Satellite Communications Systems*, John Wiley and Sons Ltd, West Sussex, PO19 IUD, England, 3rd ed., 1998, pp. 319-322.

[16]Forward, R. L., "Light-Levitated Geostationary Cylinderical Orbits," *The Journal of Astronautical Sciences*, Vol. 29, No. 1, January-March 1981, pp. 73–80.

[17]Fischer, H. and Haerting, A., "Why light-levitation geostationary cylinderical orbits are not feasible," *Journal of Astronautical Sciences*, Vol. 40, No. 3, September 1992, pp. 329–333.

[18]van de Kolk, C., "Stability of Levitated Cylinderical Orbits by Using Solar Sails," *AAS/AIAA Astrodynamics Specialist Conference, Gridwood, Alaska, AAS 99-335*, August 16-19, 1999.

[19]Ozimek, M., Grebow, D., and Howell, K., "Design of Solar Sail Trajectories with Applications to Lunar South Pole Coverage," *Journal of Guidance, Control and Dynamics*, Vol. 32, No. 6, November-December 2009, pp. 1884–1897.

[20]N. Takeichi, H. Ueno, M. O., "Feasibility Study of a Solar Power Satellite System Configured by Formation Flying," *Acta Astronautica*, Vol. 57, 2005, pp. 698–706.

[21]Hargraves, C. and Paris, S., "Dirext trajectory optimization using nolinear Programming and Collocation," *Journal of Guidance, Control and Dynamics*, Vol. 10, No. 4, 1987, pp. 338–342.

[22]Chong, E. and Żak, S., *An Introduction to Optimization*, John Wiley and Sons, New York, 1996, pp. 177-179.

[23]Pattan, B., *Satellite Systems: Principles and Technologies*, Van Nostrand Reinhold, 115 Fifth Avenue, New York, New York 10003, 1993, pp. 177-178, 180.

American Institute of Aeronautics and Astronautics